Pretargeted PET Imaging of *trans*-Cyclooctene-Modified Porous Silicon Nanoparticles

Outi Keinänen,[†] Ermei M. Mäkilä,[‡] Rici Lindgren,[‡] Helena Virtanen,[§] Heidi Liljenbäck,[§,∥]
Vesa Oikonen,[§] Mirkka Sarparanta,[†,⊥] Carla Molthoff,[#] Albert D. Windhorst,[#] Anne Roivainen,[§,∥]
Jarno J. Salonen,[‡] and Anu J. Airaksinen*,[†]

[†]Department of Chemistry - Radiochemistry, University of Helsinki, A.I. Virtasen aukio 1, 00560 Helsinki, Finland

[‡]Department of Physics and Astronomy, University of Turku, Vesilinnantie 5, 20014 Turku, Finland

[§]Turku PET Centre, University of Turku, Kiinamyllynkatu 4-8, 20520 Turku, Finland

[∥]Turku Center for Disease Modeling, University of Turku, Kiinamyllynkatu 10, 20520 Turku, Finland

[⊥]Department of Radiology, Memorial Sloan Kettering Cancer Center, 417 E 68th Street, 10065 New York, New York, United States

[#]Department of Radiology and Nuclear Medicine, VU University Medical Center, De Boelelaan 1117, Amsterdam 1081 HV, The Netherlands

S *Supporting Information*

ABSTRACT: Pretargeted positron emission tomography (PET) imaging based on bioorthogonal chemical reactions has proven its potential in immunoimaging. It may also have great potential in nanotheranostic applications. Here, we report the first successful pretargeted PET imaging of *trans*-cyclooctene-modified mesoporous silicon nanoparticles, using ^{18}F-labeled tetrazine as a tracer. The inverse electron-demand Diels−Alder cycloaddition (IEDDA) reaction was fast, resulting in high radioactivity accumulation in the expected organs within 10 min after the administration of the tracer. The highest target-to-background ratio was achieved 120 min after the tracer injection. A clear correlation between the efficiency of the in vivo IEDDA labeling reaction and the injected amount of the tracer was observed. The radioactivity accumulation decreased with the increased amount of the co-injected carrier, indicating saturation in the reaction sites. This finding was supported by the in vitro results. Our study suggests that pretargeted imaging has excellent potential in nanotheranostic PET imaging when using high-specific-activity tracers.
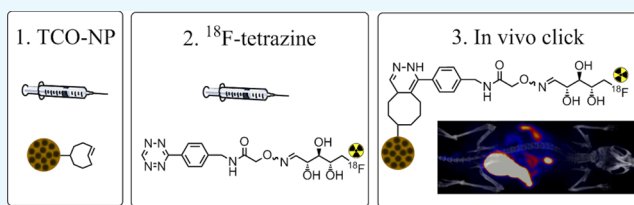
INTRODUCTION

Pretargeted molecular imaging has shown great potential in tracing monoclonal antibodies using radiolabeled reporter compounds.[1−6] The pretargeted strategy is based on separating the targeting moiety and the radiotracer from each other until most of the targeting moiety has reached its target tissue and the unbound fraction has cleared from the body. The pretargeted methodology is beneficial especially for tracing systems with slow pharmacokinetics, such as antibodies with blood half-lives in the order of days, as it allows the use of short-lived radioisotopes with clear dosimetric benefits.[2,7]

Bioorthogonal chemical reactions have been successfully applied for pretargeted positron emission tomography (PET) imaging. These reactions take place in a living biological system without interfering or being interfered by any of the system's native biochemical processes.[8,9] The most studied bioorthogonal reactions are strain-promoted alkyne azide cycloaddition (SPAAC) and the inverse electron-demand Diels−Alder cycloaddition (IEDDA) between tetrazine and a dienophile. In addition to immunoimaging, these reactions have been used very recently for tracing nanoparticles (NPs).[10−12] Pretargeted

PET imaging based on bioorthogonal chemical reactions may have great potential in nanotheranostic applications. In nanotheranostics, a drug and an imaging agent are integrated into the same nanoscale delivery system, allowing image-guided drug delivery.[13] In this way, the biodistribution and target-site accumulation of the nanotheranostic agent can be monitored noninvasively in vivo with good temporal resolution. Similarly to antibodies, peak accumulation of a nanotheranostic agent into a tumor may take several hours to several days, hampering the use of short-lived PET radioisotopes in nanotheranostic applications, especially when using methods based on the direct radiolabeling of the nanotheranostic system.

Mesoporous silicon (PSi) is a very attractive material for targeted drug delivery in nanomedicine. PSi is nontoxic and biodegradable; it degrades readily in biological environments to form silicic acid, which is excreted into urine.[14−17] The degree
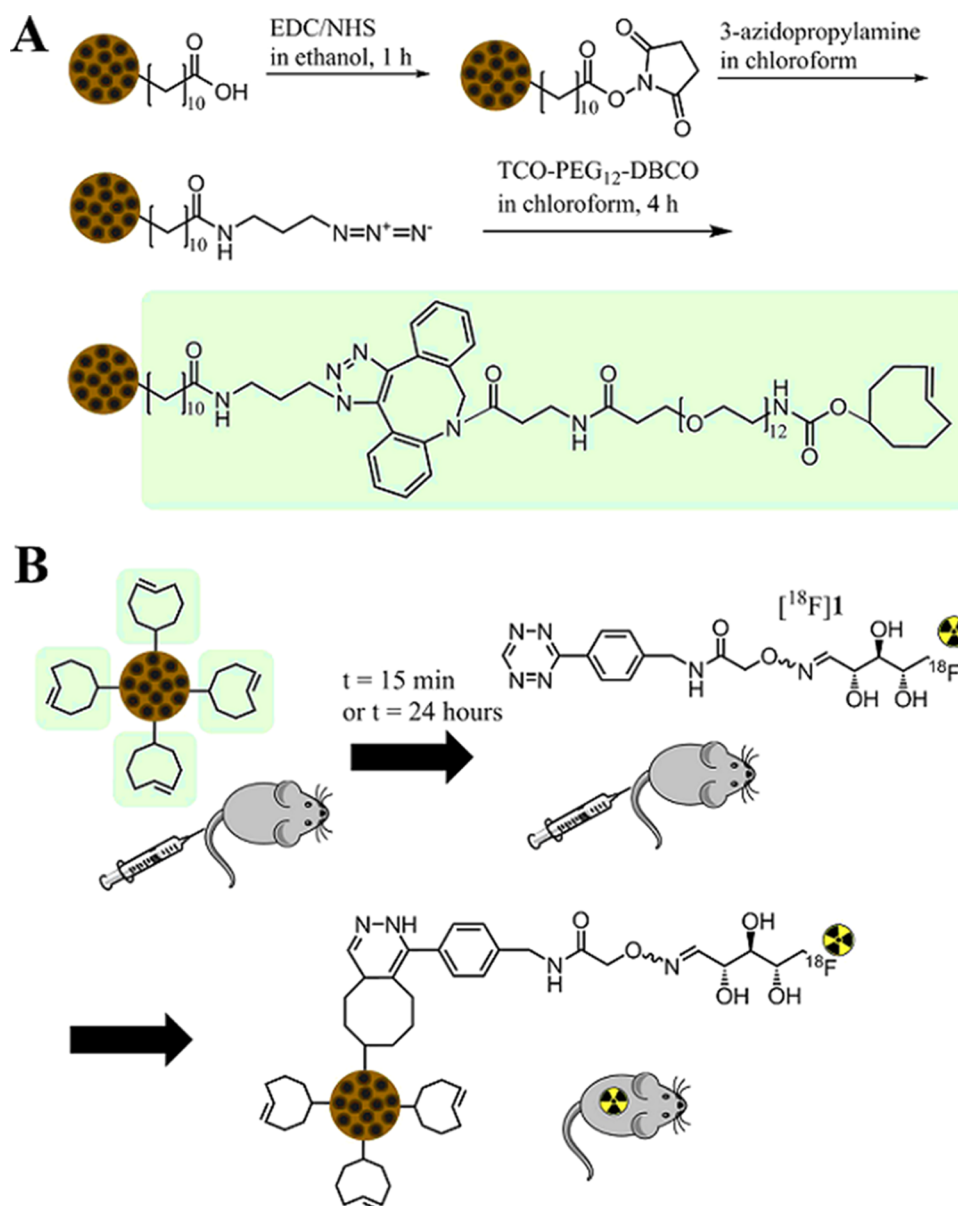
Figure 1. (A) Preparation of TCO-NPs and (B) description of the pretargeted methodology for tracing the NPs in healthy mice using [18F]**1**. TCO-NPs were administered 15 min or 24 h before the intravenous (iv) injection of [18F]**1**.

and rate of biodegradation of PSi can be modified by the porosity, pore size, and surface modification of the material.[18,19]

Recently, we have reported [18F]FDR-tetrazine ([18F]**1**) as a promising new tracer for pretargeted PET imaging.[20] Herein, we report the development of a pretargeted imaging strategy for PSi-NPs on the basis of an IEDDA reaction between [18F]**1** and *trans*-cyclooctene (TCO) (Figure 1). The IEDDA reaction follows second-order reaction kinetics, which means that the reaction rate can be increased by increasing either component of the reaction. For this reason, carrier-added tracers are generally used in IEDDA-based pretargeted methods.[21] However, tracer conditions cause competition between the tracer and the carrier on bioorthogonal reaction sites. We wanted to explore the effect of the added carrier on the in vivo IEDDA reaction by investigating the sensitivity of [18F]**1** to trace intravenously administered TCO-modified NPs in the tissues of healthy animals at different time points following NP delivery. Like other nontargeted nanomaterials, PSi exhibit

rapid and pronounced sequestration from the circulation by the organs of the mononuclear phagocyte system, the liver and spleen, in healthy subjects.[22] Nontargeted NP biodistribution in healthy mice is therefore an ideal model for pharmacokinetic studies, as the pretargeted radiotracer will be present in the liver and spleen in high amounts, facilitating region-of-interest delineation and quantitation with expected low interindividual variation. In tumor xenografts, there may be significant individual variations in tumor growth and vascularization, which may influence the NP accumulation and complicate the analysis.[23,24]

The TCO-functionalized NPs were successfully traced in vivo with the pretargeted method using [18F]**1**. The in vivo IEDDA reaction took place within 10 min after the injection of the tracer. The highest radioactivity concentration was observed in spleen and liver as typical for NPs.[23] Radioactivity concentration in the spleen, being representative of the in vivo IEDDA reaction, decreased exponentially with the

increased mass of the injected tracer. With the lowest molar amount of the tracer, approximately 25% of TCO-NPs could be traced in the spleen. Specific activity (SA) of the tracer was revealed as a very important factor for the yield of the in vivo IEDDA reaction and the sensitivity of the detection. This was confirmed in vitro, where the reaction yield decreased with the increased mass of the tracer.

■ RESULTS

Preparation and Colloidal Stability of the TCO-NPs. TCO-NPs were prepared from COOH-terminated porous silicon nanoparticles (UnTHCPSi-NP) via a stepwise procedure, first by conjugating 3-azidopropylamines on the surface through an amide bond, followed by an SPAAC reaction with *trans*-cyclooctene-PEG$_{12}$-dibenzocyclooctyne (TCO-PEG$_{12}$-DBCO) (Figure 1). Recently, it has been reported that AgNO$_3$ treatment increases stability of strained TCOs during storage.[25] Therefore, two sets of NPs were used. The first set was TCO-NPs without AgNO$_3$ treatment, and the second set was TCO-NPs with AgNO$_3$ treatment. The NPs were dissolved in a 5.4% glucose solution using a tip sonicator and left undisturbed at room temperature (RT). The AgNO$_3$ treatment was found to prevent the formation of large aggregates in the NP suspension (Table 1).

Table 1. Colloidal Stability of TCO-NPs

time point (min)	TCO-NP		Ag-TCO-NP	
	Z-average (nm)	PdI	Z-average (nm)	PdI
5	167 ± 3	0.13 ± 0.02	165 ± 2	0.15 ± 0.02
10	540 ± 29	0.44 ± 0.06	264 ± 2	0.30 ± 0.03
15	649 ± 33	0.64 ± 0.11	261 ± 8	0.27 ± 0.05
30	1297 ± 122	0.48 ± 0.05	263 ± 7	0.28 ± 0.01
60	1552 ± 22	0.46 ± 0.17	278 ± 7	0.34 ± 0.003
120	2077 ± 54	0.40 ± 0.03	280 ± 0.4	0.33 ± 0.06

Biodistribution. Compound **1** and its precursors were prepared in accordance with the previously described procedures.[20] [^{18}F]**1** was synthesized from the aminoxy-functionalized tetrazine (**5**) and [^{18}F]-5-fluoro-5-deoxy-ribose ([^{18}F]**4**) as previously described (Scheme 1).[20] To explore the influence of the concentration of [^{18}F]**1** on the IEDDA reaction, nonradiolabeled **1** was added as carrier to the synthesized [^{18}F]**1**. The TCO-NPs were intravenously injected 15 min or 24 h before the injection of [^{18}F]**1** (Figure 1B) in healthy mice. The control animals received only [^{18}F]**1**. Details of the in vivo click experiments are presented in Table 2. The

ex vivo biodistribution revealed excellent in vivo reactivity for NPs injected 15 min before the injection of [^{18}F]**1** (Figure 2). The highest radioactivity accumulation was observed in the spleen. The reaction between [^{18}F]**1** and the TCO-NPs was fast, and 11.0 ± 1.9% ID/g was observed in the spleen 15 min after the injection of [^{18}F]**1**, whereas the corresponding spleen radioactivity was 2.8 ± 0.5% ID/g for the controls (Table S3). At 60 min, the spleen radioactivity of the TCO-NP-treated animals was 9.8 ± 0.7% ID/g and only 1.0 ± 0.3% ID/g for the controls. Lower levels of radioactivity were observed in the liver (7.6 ± 2.2% ID/g) and lungs (4.6 ± 1.5% ID/g). The observed biodistribution of the in vivo labeled PSi-NPs is in good agreement with that of the preclicked NPs (Figure S4), with high accumulation in the spleen and liver as typical for nontargeted PSi-NPs.[22] The preclicked NPs showed fast clearance from the blood (0.50 ± 0.04% ID/g at 15 min), thus precluding [^{18}F]**1** reacting with TCO-NPs in the blood and then accumulating in the spleen as the major cause for the high radioactivity accumulation in the spleen with the preinjected TCO-NPs. The accumulation in lungs is typical for particles with increasing size; however, surface chemistry of the NPs may contribute as well.[26] For NPs injected 24 h before the tracer, we could not observe any in vivo click reaction between the NPs and the tracer. Clearly, the reactivity of the TCO had been lost. This is most probably due to the cis−trans isomerization or internalization of the NPs, but the dissolution of the nanomaterial itself may also contribute and cannot be completely excluded. The cycloaddition product itself is metabolically stable at least up to 2 h, as can be seen from the steady level of preclicked NPs at different time points (Figure S4). The AgNO$_3$ treatment improved the colloidal stability of the NP suspension. Therefore, we decided to use it for our further investigations with PET.

Pretargeted PET/Computed Tomography (CT) Imaging and Time−Activity Curves (TACs). The intensive binding of [^{18}F]**1** to TCO-NPs in the spleen can be clearly visualized with excellent target-to-background ratio 110−120 min after the tracer injection (Figure 3). Accumulation of [^{18}F]**1** and its radioactive metabolites can be seen in the urinary bladder, gall bladder, and intestines of both the TCO-NP-receiving animals and controls, due to urinary and hepatobiliary elimination of the tetrazine. TACs indicate a clear difference to control in the spleen standardized uptake value (SUV) within the first few minutes of observation (Figure 4). No difference in the liver was observed until [^{18}F]**1** had been washed out.

Kinetic Analysis. Logan and Patlak plots of the PET data (Figures S8 and S9) confirmed that binding in the spleen is irreversible as expected for a bioorthogonal IEDDA reaction.

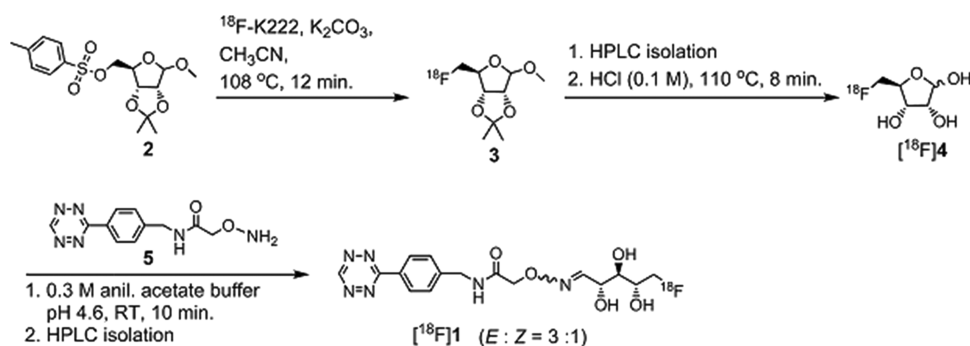**Scheme 1. Radiosynthesis of [^{18}F]1**

Table 2. Injected Amount (nmol), SA (at the Time of Injection), and Injected Radioactivity (MBq, at the Time of Injection) of [^{18}F]1 in Pretargeted Experiments with NPs

experiment	time between NP and [^{18}F]1	injected amount of NP (mg)	injected [^{18}F]1 (nmol)	SA of [^{18}F]1 (GBq/μmol)	injected dose (MBq)
TCO-NP + [^{18}F]1	15 min	0.2	0.02−117.1	0.04−207	6.9 ± 2.9
TCO-NP + [^{18}F]1	24 h	0.2	0.15−0.33	17.7−55.4	6.8 ± 2.0
control ([^{18}F]1)			0.02−0.29	6.8−554	3.4 ± 1.4
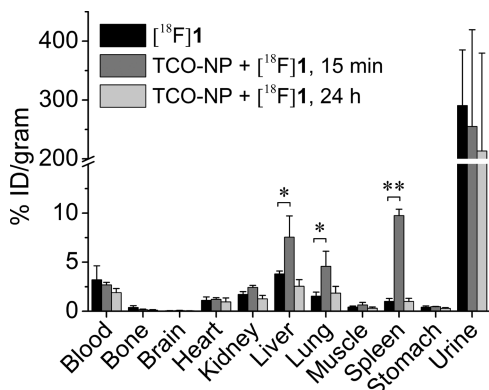
Figure 2. Biodistribution of radioactivity 60 min after the iv injection of [^{18}F]1 (black), and pretargeted TCO-NPs: NPs injected 15 min (dark gray) and 24 h (light gray) before the injection of [^{18}F]1. Values represent mean ± standard deviation (s.d.) (n = 3). *p < 0.05, **p < 0.001.
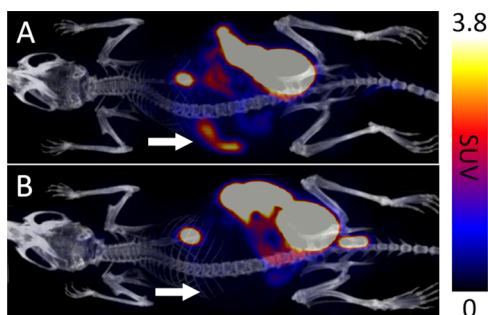
Figure 3. Representative summed PET−CT images (summed 110−120 min). (A) TCO-NPs administered 15 min before injecting [^{18}F]1. (B) Controls injected only with [^{18}F]1. The arrow indicates the location of spleen.
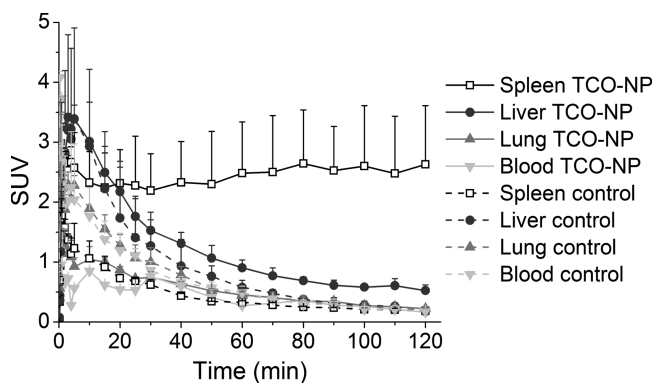
Figure 4. TACs for blood, spleen, liver, and lungs for animals injected with TCO-NPs (0.2 mg/animal) 15 min before injecting [^{18}F]1 (n = 2). The control animals were injected only with [^{18}F]1 (n = 2).

However, the results of the kinetic modeling indicated that the observed binding in the liver is reversible.

Effect of SA on the IEDDA Reaction. Significant saturation in the IEDDA reaction sites was observed in vivo, where radioactivity in the spleen (% ID/g) decreased with the injected mass of carrier 1 (Figure 5A). The saturation was exponential, and all of the TCO-NPs in the spleen could not be traced even when as little as 0.02 nmol of the tracer was injected (corresponding to an SA of 207 GBq/μmol at the time of injection). Figure 5B presents the percentage of the TCO-NPs traced in the spleen with [^{18}F]1 (calculated by formula 1) as a function of the TCO/tetrazine ratio. The percentage of traced NPs was calculated from the ex vivo biodistribution results of the pretargeted TCO-NPs and preclicked particles, as presented in formula 1. The highest percentage was achieved with the lowest injected mass of [^{18}F]1 (TCO/[^{18}F]1 ratio: 70). About 25% of TCO-NPs were traced of what could be expected on the basis of the preclicked experiment. This may be due to the limited availability and reactivity of the TCO residues in vivo. The observed saturation in the IEDDA reaction sites was further investigated in vitro using increasing amount of the NPs and two different specific activities of the tracer. Concentrations of the NPs and [^{18}F]1 were kept in the micromolar range to better simulate the conditions in vivo. The AgNO$_3$-treated NPs showed no difference compared with the regular TCO-NPs in the IEDDA reaction in vitro (Figure S2). The reaction yield decreased significantly with the increase in the concentration of the saturating carrier 1 (Figure 5C). IEDDA reaction yields of over 90% were achieved when more than 3.4 equiv of TCO were used in comparison to [^{18}F]1 (corresponds to 0.08 mg/mL of NPs).

◼ DISCUSSION

The objective of this study was to evaluate the [^{18}F]1 in pretargeted PET imaging and to explore the suitability of the pretargeted strategy for nanotheranostic applications. High-SA [^{18}F]1 was successfully used in bioorthogonal IEDDA reaction for tracing TCO-modified PSi-NPs. Logan and Patlak plots of the PET data confirmed that binding in the spleen is irreversible as expected for a bioorthogonal IEDDA reaction. However, the results of the kinetic modeling indicated that the observed binding in the liver is reversible. The IEDDA reaction itself is irreversible. The observed difference in kinetics may be due to the metabolic activity of the enzymes in the liver or faster internalization of the NPs.

It has been reported that the length of the PEG linker has an influence on the reactivity and stability of the PEGylated TCOs.[27,28] Rossin et al. reported the inactivation of antibody-bound TCO via trans−cis isomerization by copper-containing proteins. This isomerization was counteracted by shortening of the linker.[27] On the other hand, inactivation of TCO moieties on the surface of antibodies has been reported to be caused by the interactions of the hydrophobic TCO with the antibody, and this was overcome by using PEG linkers (4 or 24 subunits).[28] We used a PEG$_{12}$-linker to reduce the possible deactivation of the TCO on the thermally hydrocarbonized silicon surface and to make the TCO-moiety sterically more
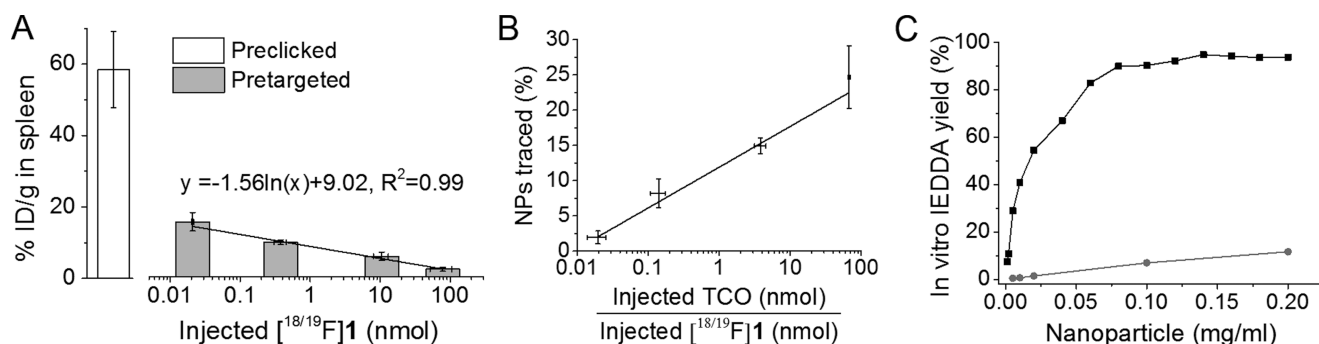
Figure 5. (A) Percentage of the injected dose per gram of spleen in preclicked and pretargeted experiments. The correlation between radioactivity accumulation in spleen (% ID/g) and the injected amount of $[^{18/19}F]\mathbf{1}$ ($y = -1.56 \ln(x) + 9.02$, $R^2 = 0.99$). (B) Percentage of the TCO-NPs traced with $[^{18}F]\mathbf{1}$ in the spleen as a function of the TCO/tetrazine ratio. (C) In vitro IEDDA yield of $[^{18}F]\mathbf{1}$ with TCO-NPs in phosphate-buffered saline (PBS) with a pH of 7.41 (7.1 nmol TCO/mg NPs, total volume: 1 mL, reaction time: 5 min). Black squares: $[^{18}F]\mathbf{1}$ (18.4 GBq/μmol) with TCO-NP; gray circles: $[^{18}F]\mathbf{1}$ (0.18 GBq/μmol) with TCO-NP.

accessible for the ^{18}F-tetrazine tracer. Our results revealed that over 70 equiv of TCO was needed to trace 25% of TCO-NPs in the spleen with $[^{18}F]\mathbf{1}$ in vivo. In contrast, 4 equiv of TCO leads to almost complete reaction in vitro. The NP concentrations in the in vitro and in vivo experiments were comparable (0.08 mg/mL in vitro and 0.12 mg/g in spleen in vivo (calculated from preclicked results, see Supporting Information (SI))). This indicates that part of the TCO groups had lost their reactivity due to either the isomerization of the groups or the formation of a plasma protein corona on the NP surface after intravenous delivery. When the NPs were administered 24 h before the tracer injection, no reaction occurred, suggesting that the activity of the TCO had decreased. Either there was not enough sterical hindrance, masking the TCO group to prevent the cis−trans isomerization in vivo, or the NPs had been completely internalized at 24 h, making the TCO groups unreachable to the ^{18}F-tetrazine tracer. Consequently, further optimization is needed for improving the stability of the dienophile on PSi surfaces and to determine the degree of PSi NP internalization to phagocytic cells over time in vivo.

Carrier-added conditions are usually preferred in the IEDDA-based pretargeted immunoimaging.[21] Duijnhoven et al. studied the phenomena with AVP04-07 diabody and ^{177}Lu.[21] They concluded that in their study optimal molar ratio in vivo was 1:1 (TCO-diabody/tracer). A decreased tracer accumulation in the tumor was observed with a lower amount of the added carrier. Under our conditions with NPs, the best results were achieved with the lowest amount of $[^{18}F]\mathbf{1}$ (0.02 nmol) and with a molar ratio of 1:0.014 (TCO/tracer). Under these conditions, we could only trace about 25% of the TCO-NPs in the spleen. Changes in TCO reactivity due to either the isomerization of the groups or the formation of a protein corona on the NP surface in plasma may have a significant influence on the observed results. Furthermore, reaction kinetics in conjunction with the fast elimination of the tracer certainly contribute.

Our study suggests that in bioorthogonal chemical reactions under tracer conditions, saturation by a carrier plays a significant role and the most efficient in vivo IEDDA labeling is achieved when high-SA tetrazine is used. The observed saturation on the IEDDA reaction sites when using a high-SA radionuclide ^{18}F may also concern the pretargeted PET imaging of antibodies, where the available TCO concentration may be even lower. However, further studies are needed to assess the

importance of the findings to the pretargeted PET imaging of antibodies.

CONCLUSIONS

The irreversible nature of binding and the limited number of TCO binding sites are very important factors of the in vivo IEDDA reactions. We achieved the best IEDDA reaction efficacy with the highest SA of the ^{18}F-labeled tetrazine $[^{18}F]\mathbf{1}$ and successfully imaged the accumulation of the modified-silicon-based NPs in vivo with PET−CT. The in vivo IEDDA reaction between the ^{18}F-tetrazine and TCOs on the surface of the PSi-NPs was fast and occurred within the first 10 min, as seen from the TACs. The yielded cycloaddition product was stable in the in vivo environment for at least 2 h. However, further optimization is still needed to maintain the high reactivity of TCO groups to permit pretargeted imaging over the course of days, which would be relevant for longer-circulating nanotheranostic agents. Our results confirm that pretargeted imaging has excellent potential in nanotheranostic PET imaging when using high-SA tracers.

EXPERIMENTAL SECTION

Unless otherwise noted, all reagents were purchased from commercial suppliers and used without further purification. All water used was ultrapure (>18.2 MΩ cm^{-1}).

Radiosynthesis. Compound $\mathbf{1}$ and its precursors were prepared in accordance with the previously described procedures.[20] $[^{18}F]\mathbf{1}$ was synthesized from the aminoxy-functionalized tetrazine ($\mathbf{5}$) and $[^{18}F]\mathbf{4}$ as previously described (Scheme 1). To explore the influence of the concentration of $[^{18}F]\mathbf{1}$ on the IEDDA reaction, nonradiolabeled $\mathbf{1}$ was added as carrier to the synthesized $[^{18}F]\mathbf{1}$. The SA was adjusted to range between 207 (no carrier added) and 0.04 GBq/μmol (maximal carrier added) at the time of injection.

Preparation of TCO-NPs. The UnTHCPSi-NPs were prepared from p+-type Si(100) wafers as previously described.[22] After fabrication and size selection, the partially COOH-terminated UnTHCPSi-NPs had a hydrodynamic diameter of 158 ± 3 nm (zeta potential: −40.5 ± 2.5). The NPs were stepwise modified to have TCO groups on the surface (Figures 1A and S1 and Table S1). To enable further chemical modification, the carboxylic acid groups were activated by N-hydroxysuccinimide/1-ethyl-3-(3-dimethylami-nopropyl) carbodiimide (NHS/EDC) cross-linking and conjugating 3-azidopropylamine through an amide bond formation

to the NPs. The TCO moieties were attached on the surface of the azide-functionalized PSi-NPs via an SPAAC reaction with TCO-PEG$_{12}$-DBCO resulting in the change of the hydrodynamic diameter of the NPs to 167 ± 3 nm (zeta potential: -39.8 ± 5.7). The amount of the resulting TCO was determined by an elemental analysis of the NPs (details in SI). In the first animal experiments, the TCO-NPs were dissolved in a 5.4% glucose solution using a vortex mixer before injecting the NPs into animals. Because of the high radioactivity accumulation in the lung (Figures S4 and S5) probably due to the formation of aggregates, for the later studies, the TCO-NPs were formulated by dissolving them in a 5.4% glucose solution using a tip sonicator. Recently, it has been reported that AgNO$_3$ treatment increases stability of strained TCOs during storage.[25] AgNO$_3$ modification was carried out by dissolving TCO-NP (2 mg) in methanol using a tip sonicator and stirring the TCO-NP suspension at RT for 1 h with AgNO$_3$ (25 mg). Then, the mixture was centrifuged (10 000g, 5 min), and the supernatant was dismissed. The particles were dispersed in water using a tip sonicator and again centrifuged (10 000g, 5 min), after which the supernatant was dismissed. The washing was repeated with 5.4% glucose solution. The particles were redispersed in the 5.4% glucose solution using a tip sonicator and injected into animals. The size and zeta potential of the resulting Ag-treated TCO-NPs were 165 ± 2 and -40.0 ± 5.1, respectively.

In Vitro Reactivity of TCO-NPs. To investigate the optimal TCO/Tz ratio for the IEDDA reaction and the saturation of the reaction sites in vitro, TCO-NPs (0.001–0.2 mg/mL) were incubated with $[^{18}F]\mathbf{1}$ of two different specific activities (18.4 and 0.18 GBq/μmol) in PBS with a pH of 7.41 (the total volume in each experiment was 1 mL). To confirm that AgNO$_3$ modification did not decrease the reactivity of the Ag-treated TCO-NPs (0.0007–0.013 mg/mL), they were tested with an SA of 19.2 GBq/μmol. The reaction was let to proceed for 5 min at RT, after which the samples were centrifuged (10 000g, 5 min) and the radioactivity of the supernatant (unreacted $[^{18}F]\mathbf{1}$) and the pellet (reacted $[^{18}F]\mathbf{1}$ with the NPs) were measured to determine the yield of the IEDDA reaction (Figure 5C).

Colloidal Stability of the NP Suspension after the AgNO$_3$ Treatment. Colloidal stability of the NP suspension after AgNO$_3$ treatment was investigated by repeated measurements using a Malvern Zetasizer Nano ZS. Two sets of NPs were used: the first set was TCO-NPs without AgNO$_3$ treatment, and the second set was TCO-NPs with AgNO$_3$ treatment. The NPs were dissolved in a 5.4% glucose solution by using a tip sonicator. The suspensions were left undisturbed at RT. In set time points, the Z-average and PdI were measured.

Animal Experiments. All animal experiments were performed in accordance with the respective national and European legislation with an approved ethical license from the National Board on Animal Experimentation (Regional State Administrative Agency of Southern Finland, Finland and VUmc, Amsterdam, the Netherlands). Details of the in vivo click experiments are presented in Table 2. The in vivo reactivity of $[^{18}F]\mathbf{1}$ was studied in healthy mice after the administration of TCO-NPs (200 μg in 5.4% glucose solution, 1.42 nmol of TCO), which were intravenously injected 15 min or 24 h before the injection of $[^{18}F]\mathbf{1}$ (6.2 ± 2.5 MBq, 0.02–117 nmol in 0.9% NaCl solution) (Figure 1B). The control animals received only $[^{18}F]\mathbf{1}$ (3.4 ± 1.4 MBq, 0.02–0.29 nmol in 0.9% NaCl solution). For NPs injected 15 min before the tracer injection, ex vivo biodistribution was studied at four time

points: 15, 30, 60, and 120 min after the injection of $[^{18}F]\mathbf{1}$. For NPs injected 24 h before the tracer injection, ex vivo biodistribution was studied in triplicate 60 min after the injection of $[^{18}F]\mathbf{1}$. The animals were sacrificed under anesthesia by cervical dislocation at designated time points after tracer administration, and samples of tissues and body fluids were collected for radioactivity measurements and weighing. The tissue samples were counted on an automated γ-counter and radioactivity decay correction was applied. The ex vivo biodistribution results were expressed as a percentage of the injected radioactivity dose per gram of tissue (% ID/g). PET imaging with Mediso nanoScan PET−CT was performed with TCO-NPs for 60 min ($n = 3$), and PET imaging with Inveon Multimodality PET−CT was performed with TCO-NPs for 120 min ($n = 2$). With CT as the anatomical reference, a quantitative PET analysis was performed by defining regions of interest (ROIs) with Inveon Research Workplace 4.1 software. The radioactivity concentration was expressed as an SUV, calculated using the average radioactivity concentration of the ROI normalized with the injected radioactivity dose and animal weight, and as TAC. The blood TAC was obtained from the left ventricle of the heart. The dynamic PET data were analyzed graphically by Logan and Patlak plots using image-derived whole-blood TACs as input function. The contribution of radioactive metabolites to the blood TAC was considered negligible[20] in this preliminary analysis.

The percentage of NPs traced in vivo in the spleen on the basis of ex vivo biodistribution was calculated by formula 1

$$\frac{\% \ ID/g_{\text{pretargeted NPs}} - \% \ ID/g_{^{18}\text{F}-1}}{\% \ ID/g_{\text{preclicked NPs}}} \times 100\% \tag{1}$$

where % ID/g$_{\text{pretargeted NPs}}$ is the percentage of injected dose per gram of radioactivity in the pretargeted TCO-NPs experiment, % ID/g^{18}$_{\text{F-1}}$ is the percentage of injected dose per gram of radioactivity in the $[^{18}F]\mathbf{1}$ control experiment, and % ID/g$_{\text{preclicked NPs}}$ is the percentage of injected dose per gram of radioactivity in the preclicked TCO-NPs experiment.

Statistical Analysis. Results of the biodistribution assays were expressed as mean $\pm$ s.d. of at least three independent experiments. Welch's t-test was used to evaluate the statistical significance, and the probabilities of $*p < 0.05$ and $**p < 0.001$ were considered statistically significant. The statistical analysis was carried out using Origin 8.6 (OriginLab Corp., Northampton, MA).

■ ASSOCIATED CONTENT

Ⓢ Supporting Information

The Supporting Information is available free of charge on the ACS Publications website at DOI: 10.1021/acsomega.6b00269.

> Tables S1−S3 and Figures S1−S9 give a more detailed description of the preparation and characterization of the NPs and animal experiments (PDF)

■ AUTHOR INFORMATION

Corresponding Author

*E-mail: anu.airaksinen@helsinki.fi. Phone: +358294150124.

ORCID Ⓞ

Ermei M. Mäkilä: 0000-0002-8300-6533
Jarno J. Salonen: 0000-0002-5245-742X
Anu J. Airaksinen: 0000-0002-5943-3105

■ ABBREVIATIONS

CCO, *cis*-cyclooctene; EDC, 1-ethyl-3-(3-dimethylaminopropyl) carbodiimide; FDR, fluorodeoxyribose; HPLC, high-performance liquid chromatography; IEDDA, inverse electron-demand Diels−Alder cycloaddition; iv, intravenous; NHS, *N*-hydroxysuccinimide; NP, nanoparticle; PBS, phosphate-buffered saline; PEG, poly(ethylene glycol); PET, positron emission tomography; PET−CT, positron emission tomography−computed tomography; PSi, porous silicon nanoparticle; RT, room temperature; ROI, region of interest; SA, specific activity; SPAAC, strain-promoted alkyne azide cycloaddition; TAC, time−activity curve; TCO, *trans*-cyclooctene; UnTHCPSi, carboxylic acid-terminated porous silicon nanoparticle

■ REFERENCES

(1) Rossin, R.; Renart Verkerk, P.; van den Bosch, S. M.; Vulders, R. C. M.; Verel, I.; Lub, J.; Robillard, M. S. In Vivo Chemistry for Pretargeted Tumor Imaging in Live Mice. *Angew. Chem., Int. Ed.* **2010**, *49*, 3375−3378.

(2) Houghton, J. L.; Zeglis, B. M.; Abdel-Atti, D.; Sawada, R.; Scholz, W. W.; Lewis, J. S. Pretargeted immunoPET of pancreatic cancer: overcoming circulating antigen and antibody internalization to reduce radiation doses. *J. Nucl. Med.* **2016**, *57*, 453−459.

(3) Meyer, J. P.; Houghton, J. L.; Kozlowski, P.; Abdel-Atti, D.; Reiner, T.; Pillarsetty, N. V.; Scholz, W. W.; Zeglis, B. M.; Lewis, J. S. F-Based Pretargeted PET Imaging Based on Bioorthogonal Diels-Alder Click Chemistry. *Bioconjugate Chem.* **2016**, *27*, 298−301.

(4) Zeglis, B. M.; Brand, C.; Abdel-Atti, D.; Carnazza, K. E.; Cook, B. E.; Carlin, S.; Reiner, T.; Lewis, J. S. Optimization of a Pretargeted Strategy for the PET Imaging of Colorectal Carcinoma via the Modulation of Radioligand Pharmacokinetics. *Mol. Pharmaceutics* **2015**, *12*, 3575−87.

(5) Zeglis, B. M.; Sevak, K. K.; Reiner, T.; Mohindra, P.; Carlin, S. D.; Zanzonico, P.; Weissleder, R.; Lewis, J. S. A pretargeted PET imaging strategy based on bioorthogonal Diels-Alder click chemistry. *J. Nucl. Med.* **2013**, *54*, 1389−96.

(6) Devaraj, N. K.; Thurber, G. M.; Keliher, E. J.; Marinelli, B.; Weissleder, R. Reactive polymer enables efficient in vivo bioorthogonal chemistry. *Proc. Natl. Acad. Sci. U.S.A.* **2012**, *109*, 4762−7.

(7) Knight, J. C.; Cornelissen, B. Bioorthogonal chemistry: implications for pretargeted nuclear (PET/SPECT) imaging and therapy. *Am. J. Nucl. Med. Mol. Imaging* **2014**, *4*, 96−113.

(8) Sletten, E. M.; Bertozzi, C. R. Bioorthogonal chemistry: fishing for selectivity in a sea of functionality. *Angew. Chem., Int. Ed.* **2009**, *48*, 6974−98.

(9) Sletten, E. M.; Bertozzi, C. R. From Mechanism to Mouse: A Tale of Two Bioorthogonal Reactions. *Acc. Chem. Res.* **2011**, *44*, 666−676.

(10) Lee, S. B.; Kim, H. L.; Jeong, H. J.; Lim, S. T.; Sohn, M. H.; Kim, D. W. Mesoporous silica nanoparticle pretargeting for PET imaging based on a rapid bioorthogonal reaction in a living body. *Angew. Chem., Int. Ed.* **2013**, *52*, 10549−52.

(11) Hou, S.; Choi, J. S.; Garcia, M. A.; Xing, Y.; Chen, K. J.; Chen, Y. M.; Jiang, Z. K.; Ro, T.; Wu, L.; Stout, D. B.; Tomlinson, J.; Wang, H.; Chen, K.; Tseng, H. R.; Lin, W. Y. Pretargeted Positron Emission Tomography Imaging that Employs Supramolecular Nanoparticles with in Vivo Bioorthogonal Chemistry. *ACS Nano* **2016**, *10*, 1417−1424.

(12) Denk, C.; Svatunek, D.; Mairinger, S.; Stanek, J.; Filip, T.; Matscheko, D.; Kuntner, C.; Wanek, T.; Mikula, H. Design, Synthesis, and Evaluation of a Low-Molecular-Weight 11C-Labeled Tetrazine for Pretargeted PET Imaging Applying Bioorthogonal in Vivo Click Chemistry. *Bioconjugate Chem.* **2016**, *27*, 1707−1712.

(13) Lammers, T.; Kiessling, F.; Hennink, W. E.; Storm, G. Nanotheranostics and Image-Guided Drug Delivery: Current Concepts and Future Directions. *Mol. Pharm.* **2010**, *7*, 1899−1912.

(14) Canham, L. T. Bioactive silicon structure fabrication through nanoetching techniques. *Adv. Mater.* **1995**, *7*, 1033−1037.

(15) Canham, L. T.; Reeves, C. L.; Newey, J. P.; Houlton, M. R.; Cox, T. I.; Buriak, J. M.; Stewart, M. P. Derivatized Mesoporous Silicon with Dramatically Improved Stability in Simulated Human Blood Plasma. *Adv. Mater.* **1999**, *11*, 1505−1507.

(16) Anderson, S. H. C.; Elliott, H.; Wallis, D. J.; Canham, L. T.; Powell, J. J. Dissolution of different forms of partially porous silicon wafers under simulated physiological conditions. *Phys. Status Solidi A* **2003**, *197*, 331−335.

(17) Hon, N. K.; Shaposhnik, Z.; Diebold, E. D.; Tamanoi, F.; Jalali, B. Tailoring the biodegradability of porous silicon nanoparticles. *J. Biomed. Mater. Res. A* **2012**, *100*, 3416−21.

(18) Salonen, J.; Kaukonen, A. M.; Hirvonen, J.; Lehto, V. P. Mesoporous silicon in drug delivery applications. *J. Pharm. Sci.* **2008**, *97*, 632−53.

(19) Salonen, J.; Lehto, V.-P. Fabrication and chemical surface modification of mesoporous silicon for biomedical applications. *Chem. Eng. J.* **2008**, *137*, 162−172.

(20) Keinänen, O.; Li, X. G.; Chenna, N. K.; Lumen, D.; Ott, J.; Molthoff, C. F.; Sarparanta, M.; Helariutta, K.; Vuorinen, T.; Windhorst, A. D.; Airaksinen, A. J. A New Highly Reactive and Low Lipophilicity Fluorine-18 Labeled Tetrazine Derivative for Pretargeted PET Imaging. *ACS Med. Chem. Lett.* **2016**, *7*, 62−66.

(21) van Duijnhoven, S. M.; Rossin, R.; van den Bosch, S. M.; Wheatcroft, M. P.; Hudson, P. J.; Robillard, M. S. Diabody Pretargeting with Click Chemistry In Vivo. *J. Nucl. Med.* **2015**, *56*, 1422−1428.

(22) Bimbo, L. M.; Sarparanta, M.; Santos, H. A.; Airaksinen, A. J.; Mäkilä, E.; Laaksonen, T.; Peltonen, L.; Lehto, V.-P.; Hirvonen, J.; Salonen, J. Biocompatibility of Thermally Hydrocarbonized Porous Silicon Nanoparticles and their Biodistribution in Rats. *ACS Nano* **2010**, *4*, 3023−3032.

(23) Duncan, R.; Sat-Klopsch, Y. N.; Burger, A. M.; Bibby, M. C.; Fiebig, H. H.; Sausville, E. A. Validation of tumour models for use in anticancer nanomedicine evaluation: the EPR effect and cathepsin B-mediated drug release rate. *Cancer Chemother. Pharmacol.* **2013**, *72*, 417−27.

(24) Ruenraroengsak, P.; Cook, J. M.; Florence, A. T. Nanosystem drug targeting: Facing up to complex realities. *J. Controlled Release* **2010**, *141*, 265−76.

(25) Murrey, H. E.; Judkins, J. C.; Am Ende, C. W.; Ballard, T. E.; Fang, Y.; Riccardi, K.; Di, L.; Guilmette, E. R.; Schwartz, J. W.; Fox, J. M.; Johnson, D. S. Systematic Evaluation of Bioorthogonal Reactions in Live Cells with Clickable HaloTag Ligands: Implications for Intracellular Imaging. *J. Am. Chem. Soc.* **2015**, *137*, 11461−75.

(26) Bertrand, N.; Leroux, J. C. The journey of a drug-carrier in the body: an anatomo-physiological perspective. *J. Controlled Release* **2012**, *161*, 152−63.

(27) Rossin, R.; van den Bosch, S. M.; Ten Hoeve, W.; Carvelli, M.; Versteegen, R. M.; Lub, J.; Robillard, M. S. Highly reactive trans-cyclooctene tags with improved stability for Diels-Alder chemistry in living systems. *Bioconjugate Chem.* **2013**, *24*, 1210−7.

(28) Rahim, M. K.; Kota, R.; Haun, J. B. Enhancing Reactivity for Bioorthogonal Pretargeting by Unmasking Antibody-Conjugated trans-Cyclooctenes. *Bioconjugate Chem.* **2015**, *26*, 352−360.